The following publication L. Wang et al., "Coherent BOTDA Using Phase- and Polarization-Diversity Heterodyne Detection and Embedded Digital Signal Processing," in IEEE Sensors Journal, vol. 17, no. 12, pp. 3728-3734, 15 June15, 2017 is available at https://doi.org/10.1109/JSEN.2017.2696043.

Coherent BOTDA using Phase- and Polarization-diversity Heterodyne Detection and Embedded Digital Signal Processing

Liang Wang, Nan Guo, Chao Jin, Kangping Zhong, Xian Zhou, Jinhui Yuan, Zhe Kang, Bin Zhou, Changyuan Yu, Haw-Yaw Tam, and Chao Lu

***Abstract*—We have proposed and experimentally demonstrated a configuration of coherent BOTDA using optical phase- and polarization-diversity heterodyne detection and embedded digital signal processing (DSP). With the unwanted probe sideband and Rayleigh scattered noise eliminated by stable electrical filtering, the in-phase and quadrature-phase heterodyne sensing signals in both x- and y- polarizations are received by the phase- and polarization-diversity coherent receiver with independent local light, and processed by the subsequent embedded DSP. The embedded DSP algorithms are designed to recover the baseband BOTDA trace for sensing and remove the intermediate frequency (IF) noise (both amplitude and phase noise) to avoid trace distortion. A spatial resolution of ~3 m and temperature accuracy of ±0.3 ºC have been achieved over 40 km sensing distance. The configuration, compatible with the detection scheme of optical coherent communication systems, is potential for future high-speed coherent BOTDA with real-time DSP designed to satisfy different requirements.**

***Index Terms*—Brillouin optical time-domain analysis (BOTDA), phase- and polarization-diversity heterodyne detection, digital signal processing**

I. Introduction

Brillouin optical time-domain analysis (BOTDA) has attracted intensive academic and industrial interest due to its promising properties for distributed temperature and strain sensing, leading to various applications in structural health monitoring, oil pipeline and power system monitoring etc [1-4]. In BOTDA systems, a pulsed pump is counter-propagating with a continuous wave (CW) probe in the optical fiber. The two beams interact through the participation of an acoustic wave and hence power transfer between them occur inside the fiber when their frequency offset is within the region of local Brillouin gain spectrum (BGS). The maximum power transfer takes place at the frequency offset equal to Brillouin frequency shift (BFS), which is linearly dependent on both the temperature and strain. The local BGS and hence BFS can be obtained by the detection of probe signal with pump-probe frequency offset scanned around BFS, and the spatial information is determined by the arrival time of the probe signal. Therefore, the temperature and/ or strain distribution along the optical fiber can be extracted accordingly.

The performance of BOTDA is related to the signal-to-noise ratio (SNR) of the sensing signal, which is limited by fiber attenuation, pump and probe power constraint due to the onset of fiber nonlinear effects and pump depletion etc [5]. Most of the research now focuses on improving the BOTDA performance and plenty of techniques have been proposed [6-14]. Among those techniques, direct detection is most commonly used although it may suffer from thermal noise of the receiver and hence set some limits on the system performance. Compared with direct detection, optical coherent detection is superior with the shot-noise limited receiver sensitivity if a local oscillator (LO) with sufficient power is provided. In 2012 A. Zornoza et al. have demonstrated a coherent self-heterodyne BOTDA by transmitting the LO together with the probe signal along the sensing fiber and achieved ~10 dB SNR improvement [15]. Then phase-modulated probe wave is utilized by the same group to improve system tolerance to non-local effect [16]. Later in 2015 Z. Li et al. have employed intensity-modulated LO transmitted with a phase-modulated probe to realize coherent BOTDA and achieved temperature sensing in 40 km distance with a spatial resolution of 3 m and ±1.8 ºC accuracy [17]. In order to avoid the distortion on the averaged BOTDA trace induced by the phase noise between the LO and the RF signal in coherent BOTDA, Z. Li et al. have proposed to use a branch of signal almost the same as the RF signal except for the additional Brillouin gain and phase shift as the LO to cancel their phase fluctuations and hence reduce the BFS decoding error to 0.4 MHz [18]. Instead of transmitting the LO and probe signal together, J. Hu et al. have proposed another configuration for coherent BOTDA where the LO with 80 MHz frequency offset from the pump is directly mixed with the probe on the photodetector and the amplitude of the

This work was supported by National Natural Science Foundation of China (NSFC) under Grant No. 61377093, 61435006 and HK GRF grant PolyU 5208/13E.

Liang Wang is with the Department of Electronic Engineering, The Chinese University of Hong Kong, Shatin, N.T., Hong Kong. (e-mail: lwang@ee.cuhk.edu.hk).

Nan Guo, Chao Jin, Kangping Zhong, Xian Zhou, Jinhui Yuan, Zhe Kang, Changyuan Yu, and Chao Lu are with the Department of Electronic and Information Engineering, The Hong Kong Polytechnic University, Kowloon, Hung Hom, Hong Kong. (e-mail: neil.nan.guo@outlook.com; jinchao1573@hotmail.com).

Bin Zhou, and Haw-Yaw Tam are with the Department of Electrical Engineering, The Hong Kong Polytechnic University, Kowloon, Hung Hom, Hong Kong.

heterodyne signal for sensing is retrieved by envelope detection using electrical spectrum analyzer (ESA) [19].

In this paper, we propose a configuration of coherent BOTDA using phase- and polarization-diversity heterodyne detection with independent LO and embedded digital signal processing (DSP). A commercial phase- and polarization-diversity coherent receiver and an independent laser as the LO are employed for the reception of the in-phase and quadrature-phase components of heterodyne sensing signal in both x- and y- polarizations, eliminating polarization mismatch between the LO and probe for coherent detection. Instead of narrowband optical filtering, the unwanted probe sideband and Rayleigh scattered noise from the pump are removed by stable electrical filtering. The heterodyne sensing signals are sampled and demodulated in a programmable oscilloscope by the designed DSP algorithms fed into it, with the unwanted intermediate frequency (IF) noise removed by the embedded DSP as well. Based on this configuration, we have demonstrated distributed temperature sensing over 40 km sensing distance with a spatial resolution of ~3 m and temperature accuracy of ±0.3 ºC. We have also discussed the effect of the phase noise and laser frequency drift on the system performance when using an independent laser as LO, which shows both of them have negligible effect on our system performance.

II. Experiment Setup and Operation

The experiment setup of the proposed coherent BOTDA configuration is shown in Fig.1 (a). The output of a CW tunable laser (TL1) operating at 1550 nm is split into two branches. The upper branch is modulated by an electro-optic modulator (EOM) biased to suppress the optical carrier and driven at a RF frequency (f_{RF} ~10.8 GHz), generating the dual-sideband (DSB) probe signal. The power of DSB probe signal is adjusted through the subsequent erbium-doped fiber amplifier (EDFA) and variable optical attenuator (VOA). On the other hand, the CW signal at the lower branch is intensity-modulated by another EOM with an extinction ratio of 40 dB, to provide pump pulses with 30 ns duration. Another EDFA is used to boost the peak power of the pump pulse and a bandpass filter (BPF) is followed to remove the amplified spontaneous emission (ASE) noise from EDFA. The peak power of the pump pulse is 20 dBm while the two probe sidebands are set at the same power level of -13 dBm. The pump pulse is delivered to the fiber under test (FUT) after passing through a polarization scrambler (PS), which is used to minimize the polarization dependent gain fluctuation. The DSB probe signal is interacting with the counter-propagating pump pulse through Brillouin scattering in FUT. For the reception of the DSB probe signal, we use Fujitsu integrated phase- and polarization-diversity coherent receiver (as shown in Fig. 1 (b)) and a EMCORE TTX1994 full band integrable tunable laser (TL2) as the LO for coherent detection. The LO has sufficient power of 13 dBm for shot-noise limited receiver sensitivity, and its wavelength is adjusted close to the lower frequency sideband of the DSB probe signal. Fig. 1 (c) depicts the frequency relationship among the pulsed pump, DSB probe and the LO. The frequency difference between the LO and the lower frequency sideband probe can be simply set and kept below 1 GHz (hundreds of MHz) in our experiment. Four electrical low-pass filters (LPF, Mini-Circuits VLFX-1350) with a passband of DC-1.35GHz are used at the four-channel outputs of the receiver, which only enables the reception of the lower frequency sideband probe, but rejects both the unwanted higher frequency sideband probe and the Rayleigh scattered noise from the pump (the frequencies of the beat signals between the two and LO are beyond ~10 GHz). Note that no narrow optical filtering is used in our configuration while stable electrical filtering is employed instead. The phase- and polarization-diversity coherent receiver firstly divides both the

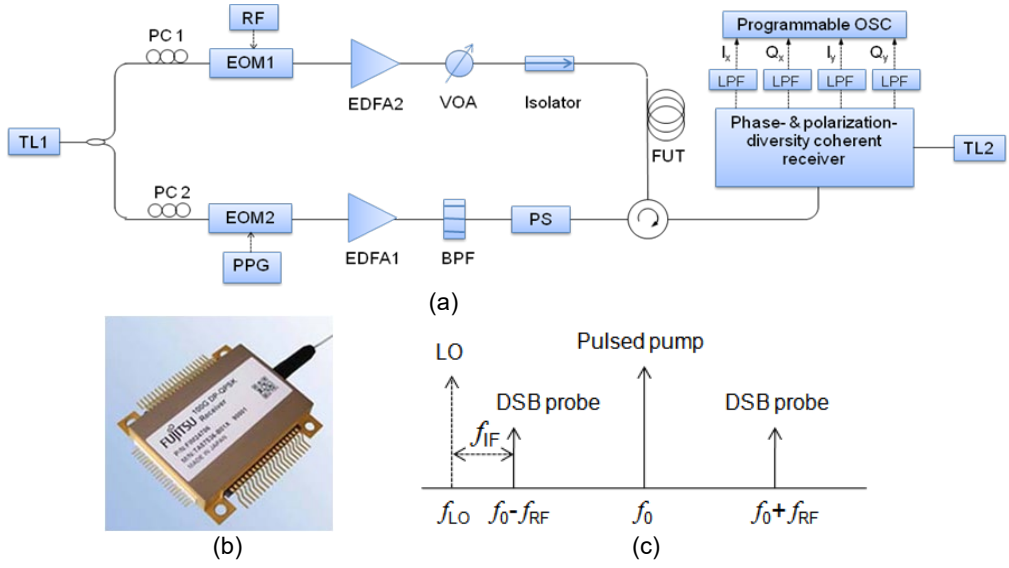

Fig. 1. (a) The experiment setup for the proposed coherent BOTDA configuration using phase- and polarization-diversity heterodyne detection with independent LO and embedded DSP; (b) Fujitsu integrated phase- and polarization-diversity coherent receiver; (c) the frequency relationship among the pulsed pump, DSB probe and the LO. TL: tunable laser; EOM: electro-optic intensity modulator; PPG: pulse pattern generator; RF: radio frequency signal generator, EDFA: erbium-doped fiber amplifier; PC: polarization controller; BPF: band pass filter; FUT: fiber under test; ISO: isolator; VOA: variable optical attenuator; PS: polarization scrambler; LO: local oscillator; LPF: low-pass filter; DSB: dual- sideband; OSC: oscilloscope.

incoming DSB probe signal and LO into x- and y-polarization components by two polarization beam splitters and then receives the beat signal between DSB probe signal and LO in both x- and y-polarizations simultaneously after they pass through two 90° optical hybrids to separate in-phase and quadrature-phase components of the beat signal, respectively. Thus the four-channel outputs of the receiver after passing through the LPF contain in-phase (I_x, I_y) and quadrature-phase (Q_x, Q_y) components of the beat signal only between the lower frequency sideband probe and the LO, in both x- and y-polarizations, respectively. The four-channel outputs can be expressed in the following [20]:

$$I_x = R\sqrt{\frac{\alpha P_s P_{LO}}{2}}\cos(2\pi f_{IF}t + \theta_s(t) - \theta_{LO}(t) + \delta) \quad (1)$$

$$Q_x = R\sqrt{\frac{\alpha P_s P_{LO}}{2}}\sin(2\pi f_{IF}t + \theta_s(t) - \theta_{LO}(t) + \delta) \quad (2)$$

$$I_y = R\sqrt{\frac{(1-\alpha) P_s P_{LO}}{2}}\cos(2\pi f_{IF}t + \theta_s(t) - \theta_{LO}(t)) \quad (3)$$

$$Q_y = R\sqrt{\frac{(1-\alpha) P_s P_{LO}}{2}}\sin(2\pi f_{IF}t + \theta_s(t) - \theta_{LO}(t)) \quad (4)$$

where P_s, P_{LO} are the powers of the lower frequency sideband probe and LO, R is the responsitivity of the photodetectors in the coherent receiver, α is the power ratio of the two polarization components, and δ is the constant phase difference between the two polarizations, $\theta_s(t)$ and $\theta_{LO}(t)$ are the phases of the lower frequency sideband probe and LO, respectively, and f_{IF} is the frequency difference between them. The four-channel electrical signals are then sampled at 3.13 GSample/s and processed according to the designed DSP algorithms fed into a 4-channel Tektronix programmable oscilloscope. In order to demodulate the heterodyne signal to the baseband and hence recover the Brillouin time-domain trace, the embedded DSP algorithms are initially designed to achieve the following two mathematic functions: quadratic sum of the four-channel electrical signals and square rooting of the result,

$$S_1 = I_x^2 + Q_x^2 + I_y^2 + Q_y^2 = \frac{1}{2}R^2 P_s P_{LO} \quad (5)$$

$$S_2 = \sqrt{S_1} = R\sqrt{\frac{1}{2}P_s P_{LO}} \quad (6)$$

We can see that with the help of polarization-diversity structure and quadratic sum operation, the baseband trace in Eq. (6) is independent of the polarization angle δ between the probe and LO, avoiding polarization fading effect existing in optical coherent detection due to the fiber birefringence [21]. Then by another DSP algorithm realizing averaging function, the signal in Eq. (6) containing the baseband Brillouin trace is averaged 2000 times to improve the SNR, and finally collected for distributed temperature monitoring.

III. Results and Discussions

(i) Preliminary experiment results

In our experiment, the FUT is a 40.2 km standard single-mode fiber (SMF) with the last 50 m section put in the oven. The last section is heated to 58 °C while the remaining fiber is kept under room temperature (22 °C). To reconstruct the BGSs, the RF frequency (f_{RF}) is swept from 10.75 to 10.90 GHz

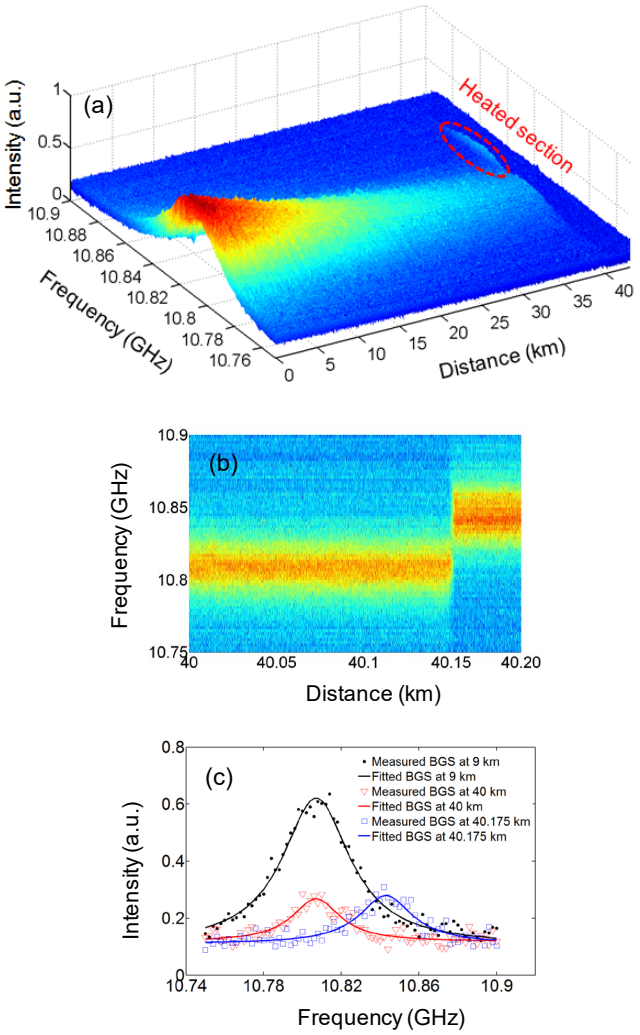

Fig. 2. (a) BGS distribution as a function of distance along the whole FUT; (b) top and zoom-in view of BGS distribution over the last 200 m fiber; (c) measured and fitted BGS at 9 km, 40 km, 40.175 km.

with a step of 2 MHz. The BGS distribution along the whole FUT measured by using our configuration is shown in Fig. 2 (a), and a top and zoom-in view of the BGS distribution over the last 200 m section of the FUT is plotted in Fig. 2 (b), where the heated section with a BFS shift is successfully detected. Fig. 2 (c) also shows the measured and fitted Brillouin gain spectra at three different locations, 9 km, 40 km and 40.175 km, in which some mismatch between the measured data and the fitted curves is observed. With Lorentzian curve fitting of the BGSs, the BFS distribution along the FUT is obtained and depicted in Fig. 3 (a). Fig. 3 (b) shows the BFS distribution near the fiber section with

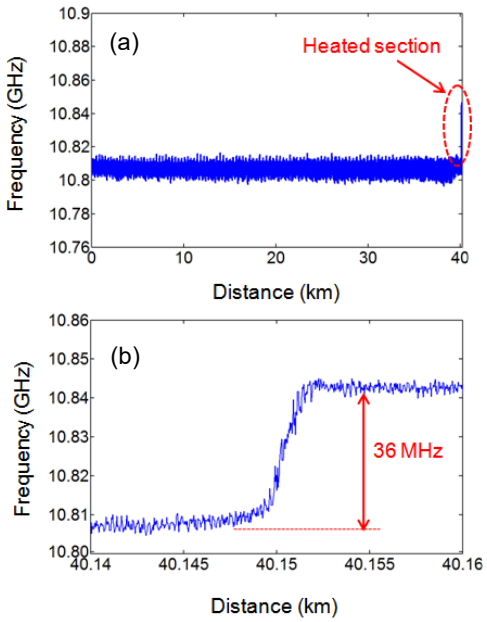

Fig. 3. (a) Measured BFS as a function of distance along the whole FUT; (b) BFS versus distance near the fiber section with temperature transition.

temperature transition, where a BFS shift is observed. The BFS of the FUT outside the oven is 10.807 GHz, while that of the heated section is found to be 10.843 GHz, showing a 36 MHz BFS shift between them. Considering the BFS temperature coefficient of ~1 MHz/ºC, the BFS shift indicates a temperature change of 36 ºC, which is in good agreement with the temperature difference between the FUT outside and inside the oven. The BFS uncertainty at the far end of FUT is calculated to be 1 MHz, which implies a temperature accuracy of ±1 ºC.

(ii) IF noise reduction by adding digital filtering function

Due to some unwanted noise, we can see plenty of the measured BGS data points deviate from the fitted BGS curves in Fig. 2 (c), even at a location not far from the beginning of the FUT, resulting in unsatisfactory quality of BGS distributions in Fig. 2 (a) and (b), and hence some fluctuations on the BFS distribution, as shown in Fig. 3 (b). One factor causing the unwanted noise may originate from the residual high frequency sideband probe and the Rayleigh scattered noise. But if we consider the LPFs used in our experiment have 40 dB attenuation for the signal with frequency above 2.6 GHz, the effect of the two should be negligible. Another factor comes from the unbalanced electrical amplifier (EA) gains between the in-phase and quadrature-phase output channels of the receiver, which are individually controlled and manually adjusted during our experiment, resulting in extra intermediate frequency (IF, f_{IF}) noise imposed on the final signal. Here we give a qualitative analysis on this case to show the extra IF components imposed on the final signal for collection. Assume ΔA and ΔB are the unbalanced EA gain-induced amplitude difference between the in-phase and quadrature-phase output channels for x- and y-polarizations, respectively, the four-channel outputs should be rewritten as:

$$I_x = R\sqrt{\frac{\alpha P_s P_{LO}}{2}}\cos(2\pi f_{IF}t + \theta_s(t) - \theta_{LO}(t) + \delta) \quad (7)$$

$$Q_x = [R\sqrt{\frac{\alpha P_s P_{LO}}{2}} + \Delta A]\sin(2\pi f_{IF}t + \theta_s(t) - \theta_{LO}(t) + \delta) \quad (8)$$

$$I_y = R\sqrt{\frac{(1-\alpha) P_s P_{LO}}{2}}\cos(2\pi f_{IF}t + \theta_s(t) - \theta_{LO}(t)) \quad (9)$$

$$Q_y = [R\sqrt{\frac{(1-\alpha) P_s P_{LO}}{2}} + \Delta B]\sin(2\pi f_{IF}t + \theta_s(t) - \theta_{LO}(t)) \quad (10)$$

Then after quadratic sum and square rooting operations by embedded DSP, the signals become:

$$\begin{aligned} S_1 &= I_x^2 + Q_x^2 + I_y^2 + Q_y^2 \\ &= \frac{1}{2}R^2 P_s P_{LO} + [2R\sqrt{\frac{\alpha P_s P_{LO}}{2}}\Delta A + \Delta A^2]\sin^2(2\pi f_{IF}t + \theta_s(t) - \theta_{LO}(t) + \delta) \\ &\quad + [2R\sqrt{\frac{(1-\alpha) P_s P_{LO}}{2}}\Delta B + \Delta B^2]\sin^2(2\pi f_{IF}t + \theta_s(t) - \theta_{LO}(t)) \end{aligned} \quad (11)$$

$$S_2 = \sqrt{S_1} = \sqrt{\frac{1}{2}R^2 P_s P_{LO} + \ldots} \quad (12)$$

Under unbalanced EA gain, we can see the final signal in Eq. (12) now contain two extra IF components with phase noise ($\theta_s(t)$-$\theta_{LO}(t)$), which result in IF noise imposed on the final signal and hence deteriorate the system performance.

In order to reduce the IF noise caused by the unbalanced EA gain, we design an additional digital filter with a passband of DC-100 MHz to filter out the IF components. The filter algorithm is inserted between those realizing quadratic sum and square rooting functions and fed into the oscilloscope as one part of the embedded DSP. Then we perform the experiment again using the new DSP algorithms but with the same experiment parameters as those in Section 3.1. In comparison

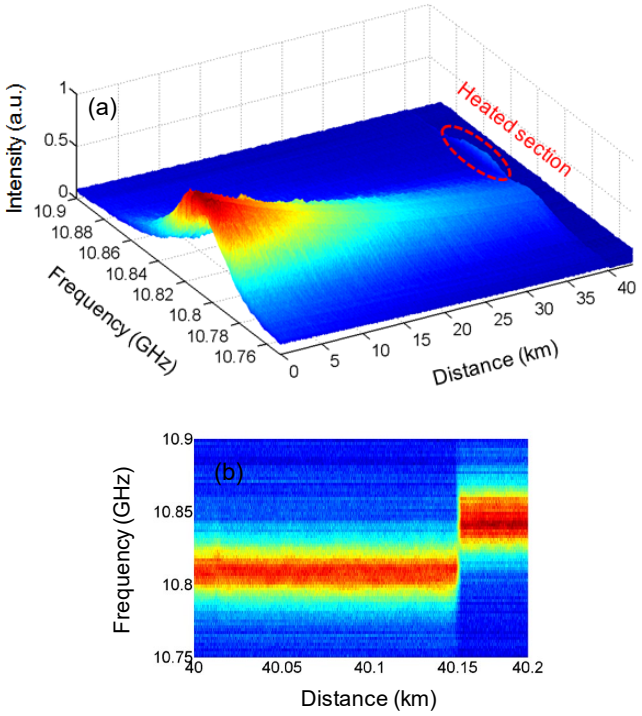

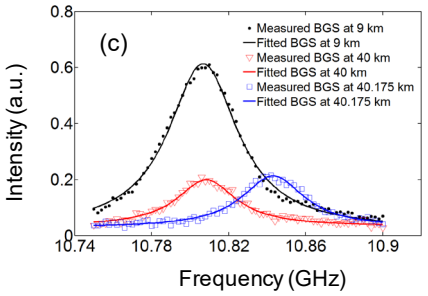

Fig. 4. (a) BGS distribution as a function of distance along the whole FUT; (b) top and zoom-in view of BGS distribution over the last 200 m fiber; (c) measured and fitted BGS at 9 km, 40 km, 40.175 km. The results are obtained using the new embedded DSP with additional digital filtering to remove the IF noise.

with the results in Fig. 2, Fig. 4 plots the BGS distributions along the FUT and the corresponding measured and fitted Brillouin gain spectra obtained from the experiment using the new embedded DSP with additional digital filtering. The BGS distributions in Fig. 4 (a) and (b) exhibit better quality and the fitted BGS curves in Fig. 4 (c) match well with the measured BGS data, even at a position near the far end of the FUT, when compared with those in Fig. 2 (c). With additional digital filtering function, the SNR near the far end of FUT is improved by 6.7 dB. By Lorentzian curve fitting, we obtain the BFS distribution along the whole FUT as plotted in Fig. 5. And Fig. 6 also shows the zoom-in view of BFS distributions within 20 m distance at three different locations, for both cases with and without digital filtering, respectively. We can see that due to the noise reduction by digital filtering, fluctuations have been reduced in Fig. 6 (b) unlike the results in Fig.6 (a). Thus the BFS uncertainty at the far end of FUT is now improved to be 0.3 MHz, corresponding to a temperature accuracy of ±0.3 °C.

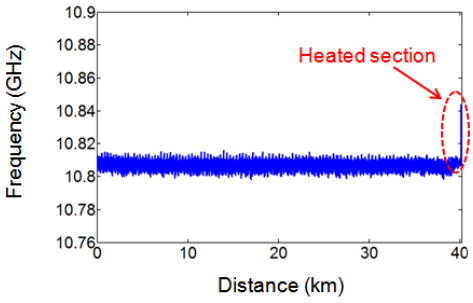

Fig. 5. Measured BFS as a function of distance along the whole FUT when digital filtering is added.

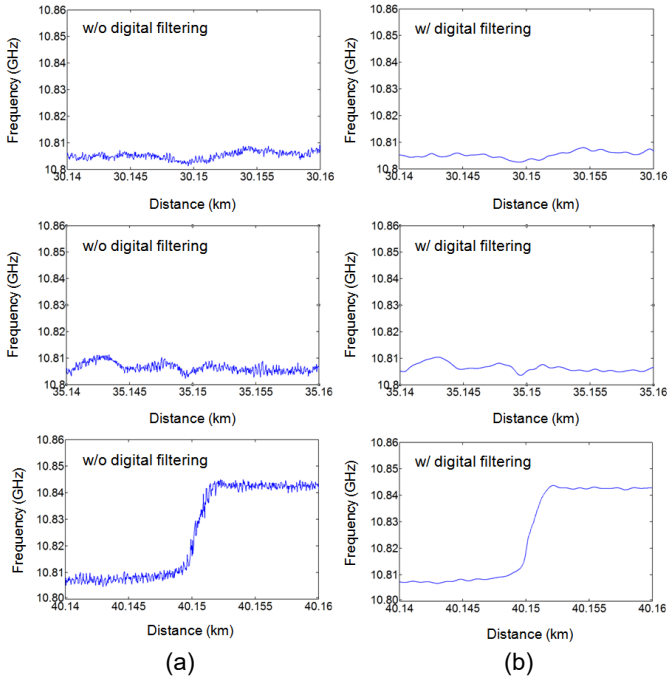

Fig. 6. Zoom-in view of BFS distributions over 20-m distance at three different locations: (a) without digital filtering; (b) with digital filtering.

(iii) Discussion

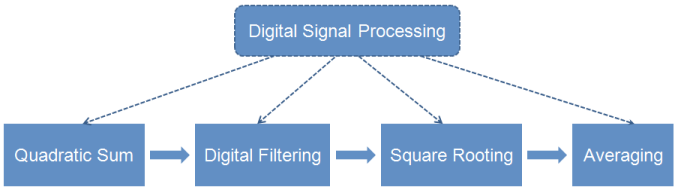

Fig. 7. Flow chart of embedded DSP and corresponding functions in our coherent BOTDA.

Fig. 7 shows the embedded DSP process in our coherent BOTDA, in which quadratic sum and square rooting functions are designed to demodulate the heterodyne signals and recover the amplitude information for sensing; while the digital filtering function together with the averaging function is designed to remove the unwanted IF noise and improve the system performance. The embedded DSP can be properly and flexibly designed to achieve various functions according to practical requirements, e.g. digital filtering function to remove IF noise in our case, or denoising function using 2D imaging processing method [22] to eliminate other kinds of noise etc. It is worth mentioning that some other existing techniques are also useful to improve the SNR. Depending on different experiment conditions, SNR improvement such as 10.3 dB by simplex coding [7, 23], 10.75 dB by self-heterodyne detection [15], 3 dB by balanced detection [24, 25], 20 dB by 2D imaging processing [22], 10-12 dB by Raman amplification, wavelet denoising and adaptive linear prediction [6, 26, 27] have been achieved and even higher improvement can also be obtained by combining several of those techniques [28]. Note that the embedded DSP is not run in a real-time manner in the oscilloscope, thus about one minute is needed to process

heterodyne signals and acquire each baseband Brillouin trace. This measurement time can be greatly reduced to several seconds with real-time DSP using a field-programmable gate array (FPGA) to replace the oscilloscope.

It is worth mentioning that we use an independent laser as LO instead of generating the LO from the same laser source. In our configuration, the LO wavelength should be set close to the lower frequency sideband of the DSB probe to facilitate the removal of both unwanted probe sideband and Rayleigh scattered noise by electrical filtering. To achieve this, it is more convenient to use an independent laser as LO to enable simple adjustment of LO wavelength and power. Otherwise, one may consider to generate the LO through relatively complicated process including optical frequency shifting, filtering and amplification, where extra optical components (e.g. modulator, filter and EDFA) will result in more cost compared with the price of an EMCORE laser used as LO. Moreover, this kind of detection configuration is compatible with the detection method for high-speed and high-capacity coherent optical communication systems, and it is potential in future integrated fiber based communication and sensing networks where optical sensing is realized in parallel with operating optical communication channels for the monitoring of external disturbances [29-31].

There are two more concerns requiring discussion: the effects of the phase noise and laser frequency drift of the LO on the system performance. Due to the use of independent laser as LO and optical fiber link transmission, the phase difference between the lower frequency sideband probe and LO ($\theta_s(t)$-$\theta_{LO}(t)$ in Eq. (1)-(4)) is time-dependent, leading to phase asynchronization or phase noise between them. The phase noise will distort the averaged trace of each channel since each trace used for cumulative average is collected under a different phase difference [18]. So we cannot average the four-channel signals (Eq. (1)-(4)) individually since they all contain the same the time-dependent phase difference. To avoid the distortions by such phase noise, we firstly obtain the BOTDA baseband time trace by quadratic sum of the four-channel electrical signals to eliminate the effect of the phase noise, and secondly average it. Even if the unbalanced EA gain results in the IF components with phase noise imposed on the final signal as expressed in Eq. (12), the DSP with additional digital filtering function ensures the elimination of the IF components and hence the phase noise. Therefore in principle the phase noise from the two lasers have negligible effect on our system performance.

Regarding the laser frequency drift, we have monitored the frequency difference (IF frequency) between the lower frequency sideband probe and LO during experiment, which is initially set around hundreds of MHz and is found to be always below 1 GHz due to the good wavelength stability of the lasers used in the experiment. The four electrical LPFs (cutoff frequency 1.35 GHz) at the four-channel outputs of the receiver only enables the reception of the lower frequency sideband probe. Thus the received signals at each output channel of the receiver can be expressed using Eq. (1)-(4). Since the four output signals have the same IF frequency which is always below the cutoff frequency of LPF, the quadratic sum of the four signals (Eq. (5)) make the IF frequency disappear if the EA gain is balanced. On the other hand, if the EA gain is unbalanced, IF frequency components exist after the quadratic sum operation (Eq. (11)), but they are removed by the digital filtering function. For both cases under balanced and unbalanced EA gain, there will be no IF frequency components in the final signal for collection. Therefore, laser frequency drift will not seriously affect the recovery of the baseband amplitude signal and system performance.

IV. Conclusion

A configuration of coherent BOTDA has been demonstrated with the use of phase- and polarization-diversity heterodyne detection and properly designed embedded DSP. The phase- and polarization-diversity structure enables the detection of the in-phase and quadrature-phase heterodyne components in both x- and y- polarizations, avoiding polarization mismatch between the probe and LO for coherent detection and facilitating the extraction of baseband BOTDA trace for sensing by subsequent DSP. The independent laser as LO simplifies the wavelength control for the removal of unwanted probe sideband and Rayleigh scattered noise by stable electrical filtering instead of narrowband optical filtering. More importantly, the embedded DSP allows flexibility in designing different functions according to practical situations, e.g. recovery of baseband BOTDA trace for sensing and reduction of unwanted IF noise (including both amplitude and phase noise) to avoid trace distortion in our case. The scheme provides a potential configuration for future high-speed coherent BOTDA with detection method compatible with coherent optical communication systems and with real-time DSP designed to meet different requirements.

References

[1] X. Bao, and L. Chen, “Recent Progress in Brillouin Scattering based Fiber Sensors,” *Sensors*, vol. 11, pp. 4152-4187, 2011.

[2] Y. Dong, P. Xu, H. Zhang, Z. Lu, L. Chen, and X. Bao, " Characterization of evolution of mode coupling in a graded-index polymer optical fiber by using Brillouin optical time-domain analysis," *Opt. Exp.*, vol. 22, no. 22, pp. 26510-26516, 2014.

[3] H. Wu, R. Wang, D. Liu, S. Fu, C. Zhao, H. Wei, W. Tong, P. P. Shum, and M. Tang, "Few-mode fiber based distributed curvature sensor through quasi-single-mode Brillouin frequency shift," *Opt. Lett.*, vol. 41, no. 7, pp. 1514-1517, 2016.

[4] D. Ba, B. Wang, D. Zhou, M. Yin, Y. Dong, H. Li, Z. Lu, and Z. Fan, " Distributed measurement of dynamic strain based on multi-slope assisted fast BOTDA," *Opt. Exp.*, vol. 24, no. 9, pp. 9781-9793, 2016.

[5] A. Dominguez-Lopez, X. Angulo-Vinuesa, A. Lopez-Gil, S. Martin-Lopez, and M. Gonzalez-Herraez, "Non-local effects in dual-probe-sideband Brillouin optical time domain analysis," *Opt. Exp.*, vol. 23, no. 8, pp. 10341-10352, 2015.

[6] F. R. Barrios, S. M. López, A. C. Sanz, P. Corredera, J. D. A. Castañón, L. Thévenaz, and M. G. Herráez, “Distributed Brillouin Fiber Sensor Assisted by First-Order Raman Amplification,” *IEEE/OSA J. Lightw. Technol.*, vol. 28, no. 15, pp. 2162 -2172, 2010.

[7] M. A. Soto, G. Bolognini, and F. Di Pasquale, "Long-range simplex-coded BOTDA sensor over 120 km distance employing optical preamplification," *Opt. Lett.*, vol. 36, no. 2, pp. 232-234, 2011.

[8] Y. Mao, N. Guo, K. YU, H. Tam, and C. Lu, "1cm spatial resolution Brillouin optical time domain analysis based on bright pulse Brillouin gain and complementary code," *IEEE Photon. J.*, vol. 4, no. 6, pp. 2243-2248, 2012.

[9] Y. Dong, C. Liang and X. Bao, "Extending the Sensing Range of Brillouin Optical Time-Domain Analysis Combining Frequency-Division Multiplexing and In-Line EDFAs," *J. Lightw. Technol.*, vol. 30, no. 8, pp. 1161-1167, 2012.

[10] Y. Dong, D. Ba, T. Jiang, D. Zhou,H. Zhang, C. Zhu, Z. Lu, H. Li, L. Chen, and X. Bao, "High-Spatial-Resolution Fast BOTDA for Dynamic Strain Measurement Based on Differential Double-Pulse and Second-Order Sideband of Modulation," *IEEE Photon. J.*, vol. 5, no. 3, pp. 2600407, 2013.

[11] A. Voskoboinik, A. W. Willner, and M. Tur, "Extending the Dynamic Range of Sweep-Free Brillouin Optical Time-Domain Analyzer," *J. Lightw. Technol.*, vol. 33, no. 14, pp. 2978-2985, 2015.

[12] F. Wang, W. Zhan, Y. Lu, Z. Yan, and X. Zhang, "Determining the Change of Brillouin Frequency Shift by Using the Similarity Matching Method," *IEEE/OSA J. Lightw. Technol.*, vol. 33, no. 19, pp. 4101 -4108, 2015.

[13] H. Chang, X. Jia, X. Ji, C. Xu, L. Ao, H. Wu, Z. Wang, and W. Zhang, "DBA-Based BOTDA Using Optical Comb Pump and Pulse Coding With a Single Laser," *IEEE Photon. Tech. Lett.*, vol. 28, no. 10, pp. 1142-1145, 2016.

[14] A. Dominguez-Lopez, Z. Yang, M. A. Soto, X. Angulo-Vinuesa, S. Martin-Lopez, L. Thevenaz, and M. Gonzalez-Herraez1, "Novel scanning method for distortion-free BOTDA measurements," *Opt. Exp.*, vol. 24, no. 9, pp. 10188-10204, 2016.

[15] A. Zornoza, M. Sagues, and A. Loayssa, "Self-heterodyne Detection for SNR Improvement and Distributed Phase Shift Measurements in BOTDA," *J. Lightwave Technol.*, vol. 30, no. 8, pp. 1066–1072, 2012.

[16] J. Urricelqui, M. Sagues, and A. Loayssa, " BOTDA measurements tolerant to non-local effects by using a phase-modulated probe wave and RF demodulation," *Opt. Exp.*, vol. 21, no. 14, pp. 17186-17194, 2013.

[17] Z. Li, L. Yan, L. Shao, W. Pan, and B. Luo, "Coherent BOTDA sensor with intensity modulated local light and IQ demodulation," *Opt. Exp.*, vol. 23, no. 12, pp. 16407-16415, 2015.

[18] Z. Li, L. Yan, L. Shao, W. Pan, B. Luo, J. Liang, H. He, and Y. Zhang, "Precise Brillouin gain and phase spectra measurements in coherent BOTDA sensor with phase fluctuation cancellation," *Opt. Exp.*, vol. 24, no. 5, pp. 4824-4833, 2016.

[19] J. Hu, X. Zhang, Y. Yao, and X. Zhao, "A BOTDA with break interrogation function over 72 km sensing length," *Opt. Exp.*, vol. 21, no. 1, pp. 145-153, 2013.

[20] I. P. Kaminow, T. Li, and A. E. Willner, *Optical Fiber Telecommunications V B: Systems and Networks*, Chapter 3, Elsevier, 2008.

[21] Y. Cao, Q. Ye, Z. Pan, H. Cai, R. Qu, Z, Fang, H. Zhao, "Mitigation of polarization fading in BOTDR sensors by using optical pulses with orthogonal polarizations," *Proc. of SPIE, vol. 9157, pp. 915764, 23rd International Conference on Optical Fibre Sensors*, Santander, Spain, June 2014.

[22] M. A. Soto, J. A. Ramírez, and L. Thévenaz, "Intensifying the response of distributed optical fibre sensors using 2D and 3D image restoration," *Nat. Commun.*, vol. 7, pp. 10870, 2016.

[23] M. A. Soto, G. Bolognini, F. D. Pasquale, and L. Thévenaz, "Simplex-coded BOTDA fiber sensor with 1 m spatial resolution over a 50 km range," *Opt. Lett.*, vol. 35, no. 2, pp. 259-261, 2010.

[24] A. Domínguez-López, A. López-Gil, S. Martín-López, and M. González-Herráez, "Signal-to-Noise Ratio Improvement in BOTDA Using Balanced Detection," *IEEE Photon. Tech. Lett.*, vol. 26, no. 4, pp. 338-341, 2014.

[25] A. Minardo, A. Coscetta, L. Zeni, and R. Bernini, "High-Spatial Resolution DPP-BOTDA by Real-Time Balanced Detection," *IEEE Photon. Tech. Lett.*, vol. 26, no. 12, pp. 1251-1254, 2014.

[26] M. Farahani, M. Wylie, E. Castillo-Guerra, and B. Colpitts, "Reduction in the number of averages required in BOTDA sensors using wavelet denoising techniques," *J. Lightwave Technol.* vol. 30, no. 8, pp. 1134–1142, 2012.

[27] M. A. Farahani, E. Castillo-Guerra, and B. G. Colpitts, "Acceleration of measurements in BOTDA sensors using adaptive linear prediction," *IEEE Sensors J.*, vol. 13, no. 1, pp. 263–272, 2013.

[28] M. A. Soto, X. Angulo-Vinuesa, S. Martin-Lopez, S. Chin, J. D. Ania-Castanon, P. Corredera, E. Rochat, M. Gonzalez-Herraez, and L. Thevenaz, "Extending the Real Remoteness of Long-Range Brillouin Optical Time-Domain Fiber Analyzers," *J. Lightwave Technol.* vol. 32, no. 1, pp. 152–162, 2014.

[29] H. F. Martins, K. Shi, B. C. Thomsen, S. M. Lopez, M. G. Herraez, and S. J. Savory, "Real time dynamic strain monitoring of optical links using the backreflection of live PSK data," *Opt. Exp.*, vol. 24, no. 19, pp. 22303-22318, 2016.

[30] J. Hu, X. Chen, Z. Ren, S. Shi, K. Yan, Y. Zhang, "A Novel In-Service OTN Fiber Link Monitoring Scheme using Correlation-Based OTDR," *Asia Communications and Photonics Conference 2016*, Wuhan, Hubei, China, November 2016, paper *AF2A.110.*

[31] G. C. Amaral, J. D. Garcia, L. E. Y. Herrera, G. P. Temporao, P. J. Urban, and J. P. Weid, "Automatic Fault Detection in WDM-PON With Tunable Photon Counting OTDR," *IEEE/OSA J. Lightw. Technol.*, vol. 33, no. 24, pp. 5025 -5031, 2015.